SPECIAL
State of the Science of Precipitation
COLLECTION

A Real-Time Algorithm for the Correction of Brightband Effects in Radar-Derived QPE

JIAN ZHANG

NOAA/OAR/National Severe Storms Laboratory, Norman, Oklahoma

YOUCUN QI

Nanjing University of Information Science and Technology, Nanjing, China, and Cooperative Institute for Mesoscale Meteorological Studies, University of Oklahoma, Norman, Oklahoma

(Manuscript received 11 August 2009, in final form 17 March 2010)

ABSTRACT

The bright band (BB) is a layer of enhanced reflectivity due to melting of aggregated snow and ice crystals. The locally high reflectivity causes significant overestimation in radar precipitation estimates if an appropriate correction is not applied. The main objective of the current study is to develop a method that automatically corrects for large errors due to BB effects in a real-time national radar quantitative precipitation estimation (QPE) product. An approach that combines the mean apparent vertical profile of reflectivity (VPR) computed from a volume scan of radar reflectivity observations and an idealized linear VPR model was used for computational efficiency. The methodology was tested for eight events from different regions and seasons in the United States. The VPR correction was found to be effective and robust in reducing overestimation errors in radar-derived QPE, and the corrected radar precipitation fields showed physically continuous distributions. The correction worked consistently well for radars in flat land regions because of the relatively uniform spatial distributions of the BB in those areas. For radars in mountainous regions, the performance of the correction is mixed because of limited radar visibility in addition to large spatial variations of the vertical precipitation structure due to underlying topography.

1. Introduction

The National Mosaic and the next-generation quantitative precipitation estimation (Q2) system (NMQ; more information available online at http://nmq.ou.edu; Seo et al. 2005; Vasiloff et al. 2007) is a real-time test bed for the research, development, and evaluation of national multisensor precipitation products. One of the NMQ products is the radar-based precipitation estimate that uses adaptive *Z–R* relationships (Xu et al. 2008). The NMQ precipitation products have been under real-time evaluations at several river forecast centers. One of the issues found with the NMQ radar-based precipitation product is the overestimation of precipitation associated with bright band (BB). The bright band is a layer of enhanced reflectivity due to melting of aggregated snow (Fig. 1). The phenomenon has been recognized near the beginning of radar meteorology (e.g., Ryde 1947; Austin and Bemis 1950; Wexler and Atlas 1956; Lhermitte and Atlas 1963), and many recent studies have been able to identify the BB layer from operational Weather Surveillance Radar-1988 Doppler (WSR-88D) radar observations (e.g., Gourley and Calvert 2003; Zhang et al. 2008).

Figure 1 shows five events where radar-derived quantitative precipitation estimation (QPE) had different types of BB-related overestimation. The first was a typical cool season stratiform rain event occurred on 15 November 2008 in the northeast United States (Figs. $1a_1$–$1c_1$). The BB layer was clearly defined and its bottom was well above the ground (Fig. $1c_1$), and overestimations of 50%–200% were found in a northeast–southwest-oriented band where the radar beam intersected the BB layer. The second was a springtime squall-line system that occurred on 27 May 2008 in the southern plains (Figs. $1a_2$–$1c_2$). An area of overestimation was found in

Corresponding author address: Jian Zhang, NSSL/WRDD, 120 David L. Boren Blvd., Norman, OK 73072.
E-mail: jian.zhang@noaa.gov

DOI: 10.1175/2010JHM1201.1

© 2010 American Meteorological Society

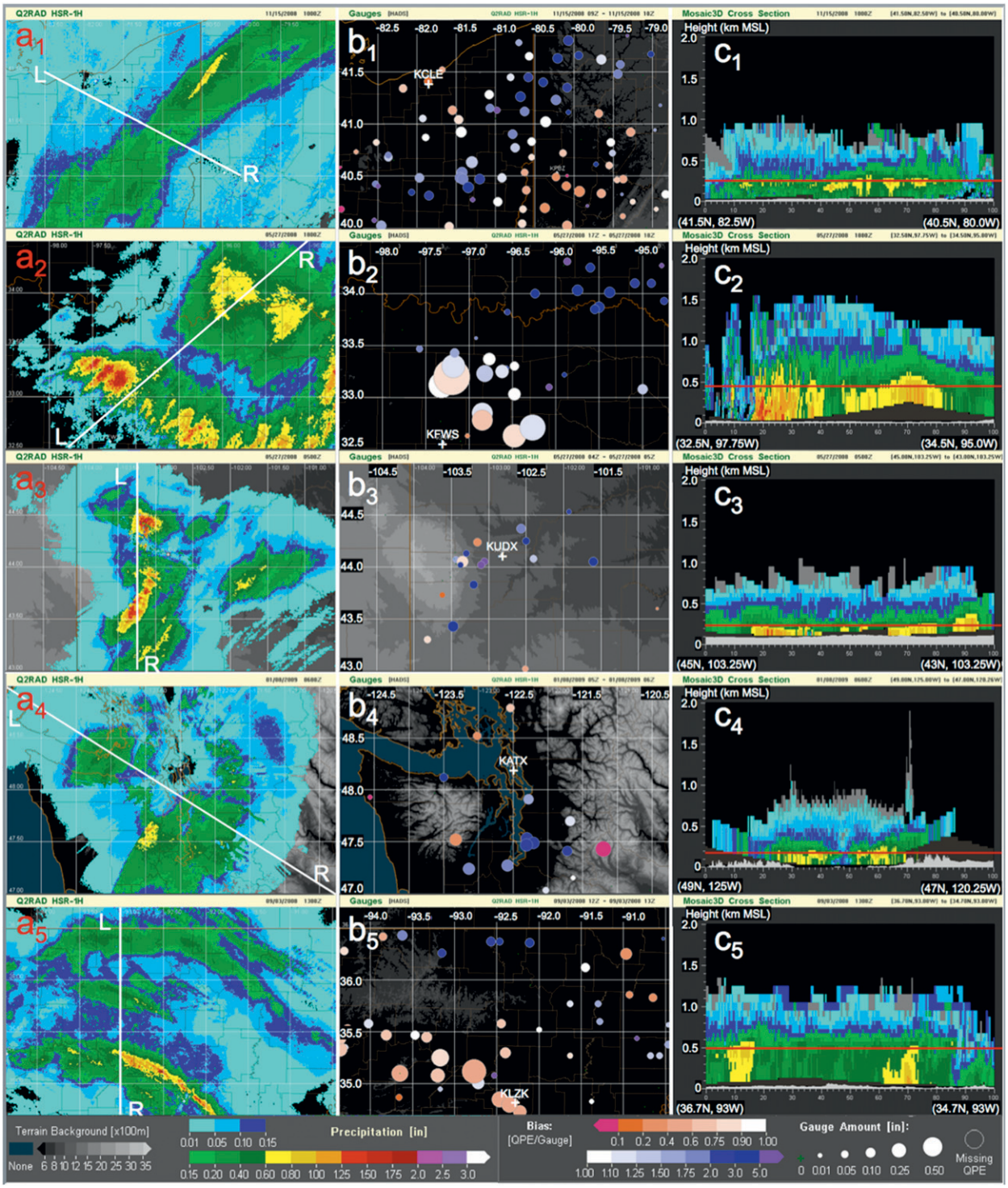

FIG. 1. Example products from the real-time NMQ system for different regions: (column a) 1-h radar rainfall estimates, (column b) ratio bias between radar and gauge 1-h rainfall products (blue dots indicating radar overestimation and red indicating radar underestimation); and (column c) vertical cross sections along the white lines in (a). The white letters "L" and "R" indicate the left and right ends of the cross sections in (c). The red lines in (c) represent the 0°C height level at the radar site. The location and time of the events were (from top to bottom) for KCLE at 1000 UTC 15 Nov 2008, KFWS at 1800 UTC 27 May 2008, KUDX at 0500 UTC 27 May 2008, KATX at 0600 UTC 8 Jan 2009, and KLZK at 1300 UTC 3 Sep 2008.

the trailing stratiform rain (Figs. $1a_2$ and $1b_2$) due to a deep BB layer (Fig. $1c_2$) that most likely contained large melting snow aggregates. The third was a heavy snow–rain mixed event that also occurred on 27 May 2008, but in the northern plains with a BB that was located near the surface (Fig. $1c_3$). The bottom of the BB was not well defined and there were evident spatial variations of the BB layer, probably due to impacts by the underlying terrain. The fourth was a heavy precipitation event that occurred on 8 January 2009 in the mountainous northwest Pacific region, with overestimation associated with a BB (e.g., near 47.5°N, 122.3°W; Fig. $1b_4$) as well as underestimation associated with blockage/overshooting (e.g., near 47.5°N, 123.4°W; Fig. $1b_4$). The BB feature coexisted with orographically enhanced precipitation (Fig. $1c_4$). The fifth was the Tropical Storm Gustav event on 3 September 2008 in the southeast, where overestimations associated with a BB (near northern boundary of the domain; Fig. $1b_5$) was accompanied with underestimations associated with tropical precipitation (southwest of the domain; Fig. $1b_5$). The north–south vertical cross section (Fig. $1c_5$) revealed a BB layer to the north and a typical warm rain core to the south.

The bright band causes significant overestimation in radar precipitation estimates if appropriate correction is not applied. To mitigate radar precipitation errors associated with bright band and also with the ice region above BB, both of which are due to nonuniform vertical profiles of reflectivity (VPRs), many methods have been proposed (e.g., Koistinen 1991; Joss and Lee 1995; Andrieu and Creutin 1995; Kitchen et al. 1994; Smyth and Illingworth 1998; Westrick et al. 1999; Vignal et al. 1999, 2000; Seo et al. 2000; Vignal and Krajewski 2001; Germann and Joss 2002; Bellon et al. 2005; and references therein). These correction methods can be approximately classified into four types according to the VPRs used in the correction: 1) climate VPR; 2) mean observed volume VPR, which is usually computed from volumetric radar observations at close ranges and then applied for VPR corrections at far ranges; 3) retrieved local VPR; and 4) conceptual model or parameterized VPRs.

Advantages and disadvantages associated with each type of VPRs have been discussed in previous studies including Joss and Lee (1995), Vignal et al. (2000), Vignal and Krajewski (2001), and Germann and Joss (2002). Furthermore, Germann and Joss (2002) provided a comprehensive review of temporal and spatial scales of various VPR correction techniques. In summary, climate VPRs are obtained from radar observations averaged over certain spatial area (e.g., a radar umbrella or within certain precipitation regimes) and over a long time period (e.g., on the order of days or a year). These VPRs do not represent temporal and spatial variations of the vertical structure of precipitation. They are often used as default VPRs only when real-time and smaller-scale (hourly or shorter) VPRs are not available. Mean volume scan VPRs are obtained from multiple elevations of one or several volume scan data [(e.g., over an hour, or, ''mesobeta'' scale as described in Germann and Joss 2002)]. These VPRs can better capture temporal variations of the vertical structure of precipitation as compared to the climate VPRs, and are widely used in previous studies, especially for operations (e.g., Koistinen 1991; Joss and Lee 1995; Germann and Joss 2002). The mean volume scan VPRs are usually assumed to have the same structure over a radar umbrella, thus neglecting spatial variations of vertical precipitation profiles. Andrieu and Creutin (1995) proposed a sophisticated inversion scheme to filter radar sampling effects (i.e., beam broadening as a function of range) and retrieved a mean VPR over the radar domain from two elevation angles. The scheme was later generalized by Vignal et al. (1999) to retrieve local VPRs over a small area of 20 km × 20 km using multiple elevation angles and was evaluated on Swiss (Vignal et al. 2000) and U.S. (Vignal and Krajewski 2001) radar data. Both evaluations showed that the local VPR approach provided more improvements in radar-derived QPE than the mean volume scan VPRs. However, the local VPR approach is relatively expensive computationally and is not easily implemented for operational applications. Thus, an alternative VPR approach based on idealized VPR models with a reduced number (i.e., 5–6) of physically based parameters has been adapted by many studies (e.g., Kitchen et al. 1994; Kitchen 1997; Matrosov et al. 2007; Tabary 2007).

Kitchen et al. (1994) proposed a local idealized VPR for each radar pixel and determined parameters of the VPR using radar, surface observation, and satellite infrared data. This scheme was then extended by Kitchen (1997) for improving radar rainfall estimates in a complex terrain. Smyth and Illingworth (1998) applied similar parameterized VPR correction to radar-derived QPE, but only to stratiform precipitation, which was segregated from convective regions. A more recent work by Matrosov et al. (2007) applied correction using an idealized VPR to X-band polarimetric radar data and a reduced standard deviation of radar rainfall estimation with respect to surface rain gauge observations. Parameters for the VPR model were determined from a dual-polarization variable (copolar correlation coefficient) radar and from some previous results based on vertically pointing radars (Fabry and Zawadzki 1995). These parameterized VPR models were shown to be useful in complex terrain where radar-observed VPR had limited coverage in the vertical. And they are computationally efficient and easy to implement.

The main objective of the current study is to develop a method that automatically corrects for large errors due to brightband effects in the real-time NMQ radar-derived QPE product. Therefore, both product accuracy and computational efficiency are important. The correction for underestimations associated with radar beam sampling in the ice region will be addressed in a separate study. An approach that combines the mean volume scan VPR and the idealized VPR techniques was adapted based on the following considerations:

1) The mean volume scan VPR approach is used because of its computational simplicity and efficiency. In their study, Vignal et al. (2000) showed that the mean VPR could reduce the fractional standard error (FSE) in radar-derived QPE from noncorrected 41% to 25%. Using local VPRs further reduces the FSE to 23%. Vignal and Krajewski (2001) found similar results in that the performance of the mean VPR and the local VPR schemes was similar while the latter provided consistently better results. However, the local VPR correction is not currently feasible to run in real time for a national domain with over 140 radars.
2) VPRs in the current study are computed from single volume scan of radar data instead of averaging multiple volume scans over a time period. This simplifies computations by avoiding the need for time associations. Experience with 3 yr of radar data in the NMQ system indicated that the spatial average in a volume scan provided stable VPRs when there was relatively widespread precipitation. When the precipitation is scattered, representative VPRs would be hard to obtain and a VPR correction would be ineffective because of large variations associated with the vertical structure in scattered precipitation.
3) An idealized VPR model is used in the current study with a small number of parameters that can be derived from meteorological information and from radar volume data. In addition to its simplicity, the idealized VPR model can be used to correct for radar precipitation overestimation associated with a bright band near the ground (e.g., the third event in Fig. 1). Under this situation, a representative reference reflectivity below the BB cannot be obtained from radar observations and traditional VPR correction approaches cannot work properly. An extrapolated VPR based on some parameterizations is needed for the correction.
4) Parameters in the idealized VPR model are dynamically adjusted using real-time radar observations as well as environmental data. This can help obtain more representative VPRs than idealized models with predefined parameters. The latter approach could result in discontinuities in the corrected radar fields when the predefined parameters did not represent the real-time BB distribution.

Descriptions of the basic correction method and some examples demonstrating the correction procedure are provided in the next section. Case study results for eight events representing various geographical regions and different seasons in the United States are presented in section 3. A summary and discussion of future work follows in section 4.

2. Methodology

Since the current VPR correction scheme is for brightband correction, it assumes that the 0°C height (or freezing level) is above the ground. In other words, the scheme is designed for liquid precipitation at this point, not for snow. If the 0°C height (usually obtained from a radio sounding or from a model temperature profile) is at or below the ground, then no VPR correction will be applied. The correction procedure includes four major steps that are presented below.

a. Convective–stratiform segregation and brightband area delineation

Because of large differences between the vertical structure of convective–stratiform precipitation (e.g., Smyth and Illingworth 1998; Steiner et al. 1995; Zhang et al. 2008), it is important to segregate the two types of precipitation before a VPR correction is applied (Smyth and Illingworth 1998). In the current study, convective–stratiform precipitation segregation was initially based on the same technique as in Zhang et al. (2008). However, tests with a few squall-line events (including the second event in Fig. 1) indicated that the technique misidentified some regions in the trailing stratiform precipitation as convective, due to that the reflectivities at −10°C height in those regions was higher than 30 dBZ. Therefore, a different method based on the vertically integrated liquid water (VIL; Greene and Clark 1972) was used instead.

The VIL is calculated from a single radar volume scan reflectivity data (spatial resolution is ~1 km × 1° and temporal resolution is ~5 min) as follows:

$$\mathrm{VIL} = \sum_k \mathrm{VILpar}_k, \tag{1}$$

where VILpar_k is the VIL within a specific (k^{th}) tilt at a given gate:

$$\mathrm{VILpar} = \mathrm{LW} \times \mathrm{DB}. \tag{2}$$

Here LW and DB are computed by Eqs. (3) and (4) below, respectively:

$$\mathrm{LW} = 3.44 \times 10^3 \mathrm{ZE}^{4/7}, \tag{3}$$

$$\mathrm{DB} = \begin{cases} \mathrm{BH}[\theta_{k_{\mathrm{top}}} + 0.5\mathrm{BW}] - \mathrm{BH}[0.5(\theta_{k_{\mathrm{top}}} + \theta_{k_{\mathrm{top}}-1})] & k = k_{\mathrm{top}} \\ \mathrm{BH}[0.5(\theta_{k+1} + \theta_k)] - \mathrm{BH}[0.5(\theta_k + \theta_{k-1})] & 1 < k < k_{\mathrm{top}}, \\ \mathrm{BH}[0.5(\theta_2 + \theta_1)] & k = 1 \end{cases} \tag{4}$$

where LW is the liquid water content associated with a particular value of reflectivity (kg km^{-3}). The quantity DB is the depth of a radar beam as a function of range (km), ZE is the effective radar reflectivity factor (mm^6 m^{-3}) within a radar sample volume BW is the angular width of the radar beam between the half-power points (3 dB; BW equals 0.95° for WSR-88D), BH represents the beam center height for a given elevation angle and range under the standard atmospheric refraction conditions, and θ_k is the elevation angle at the kth tilt.

The convective–stratiform segregation is applied to single radar data in the polar coordinates. If the VIL at any range–azimuth bin is greater than a threshold (default = 6.5 kg km^{-2}), then the gate is classified as convective. Otherwise, it is classified as being stratiform. The VIL threshold is an empirical parameter and the initial value was based on subjective analyses of composite reflectivity (i.e., the maximum reflectivity in a grid column) fields from several squall-line events in the central United States during 2008 and 2009. This method was found to produce similar results as those in Zhang et al. (2008) while minimizing the misidentification of convection in the trailing stratiform precipitation behind squall lines.

The stratiform area is further divided into two parts: one is the BB affected area (BBA), and another is not. The BBA is delineated as areas (i) within a first-guess apparent BB top (default = 0°C height + D_1) and apparent BB bottom (default = 5 km below the apparent BB top) boundaries; and (ii) with composite reflectivities greater than a predefined threshold, Z_{BB}. The parameter D_1 is the difference between height of the center of the lowest beam where it intersects the 0°C level and height of the bottom (i.e., the 3-dB beamwidth) of the lowest beam where the center of the beam intersects the 0°C level. Therefore, D_1 is dependent on the beamwidth of the lowest tilt at the height of the freezing level. The higher the melting layer, the farther the range where the lowest tilt intersects the BB, and the larger the D_1. The background 0°C level is obtained from a model temperature sounding at the radar location.

The low apparent BB bottom boundary (5 km below the top) were selected to encompass the largest possible ranges that may be potentially impacted by a BB, including those associated with melting snow aggregates within the trailing stratiform precipitation behind squall lines (e.g., Fig. 1c$_2$), and for varying melting layer (0°C) heights in space and in time. Here Z_{BB} is a minimum reflectivity threshold for apparent BB observations, and the default value is set to 30 dBZ based on analyses of eight widespread precipitation events (Table 2) from different areas in the contiguous United States (CONUS). In the current study, the VPR is only derived and applied to the BBA rather than to the whole radar coverage. Oftentimes, the bright band does not uniformly distribute in all the sectors of a radar's observational umbrella. If a single mean VPR was computed from the whole radar volume scan, then the brightband peak intensity in the VPR may be reduced due to contributions from non-BB data. On the other hand, if this one VPR was applied for corrections everywhere, then there would be undercorrections in brightband areas and overcorrections in non-BB areas. By segregating BBA from the rest of the precipitation, the overestimation due to BB can be most effectively corrected.

Figure 2 shows an example of the convective–stratiform segregation and the BBA delineation for a squall-line event observed by the KFWS radar. There was a large area of enhanced reflectivity (see red circle in Fig. 2a), likely due to melting snow aggregates, in the trailing stratiform precipitation behind the squall line. The convective–stratiform segregation successfully identified the majority of the convective rainband (red area, Fig. 2b) and the trailing stratiform area (blue area, Fig. 2b). The correction was applied to the stratiform region with reflectivity higher than 30 dBZ (red circled area, Fig. 2a). However, the edges of the convective rainbands were also identified as stratiform (Figs. 2b versus 2a) due to their relatively low VIL values (Fig. 2c). Precipitation estimates in some convective regions (i.e., red square in Fig. 2a) were inappropriately adjusted (reduced) because they were in the same range as the BB. Examination of the VIL field (Fig. 2c) indicates that VIL values in strong BB areas can be as high as those in regions around convective cores. But VIL gradients around convective cores appear to be larger than in the BB area. Thus, expansion of convective cores based on spatial VIL distributions may further refine the convective–stratiform segregation and reduce such errors. Refinements of the convective–stratiform segregation will continue in future work.

b. *Parameterized BB VPRs*

Since the current study is focused on stratiform precipitation, it is assumed that the vertical structure of

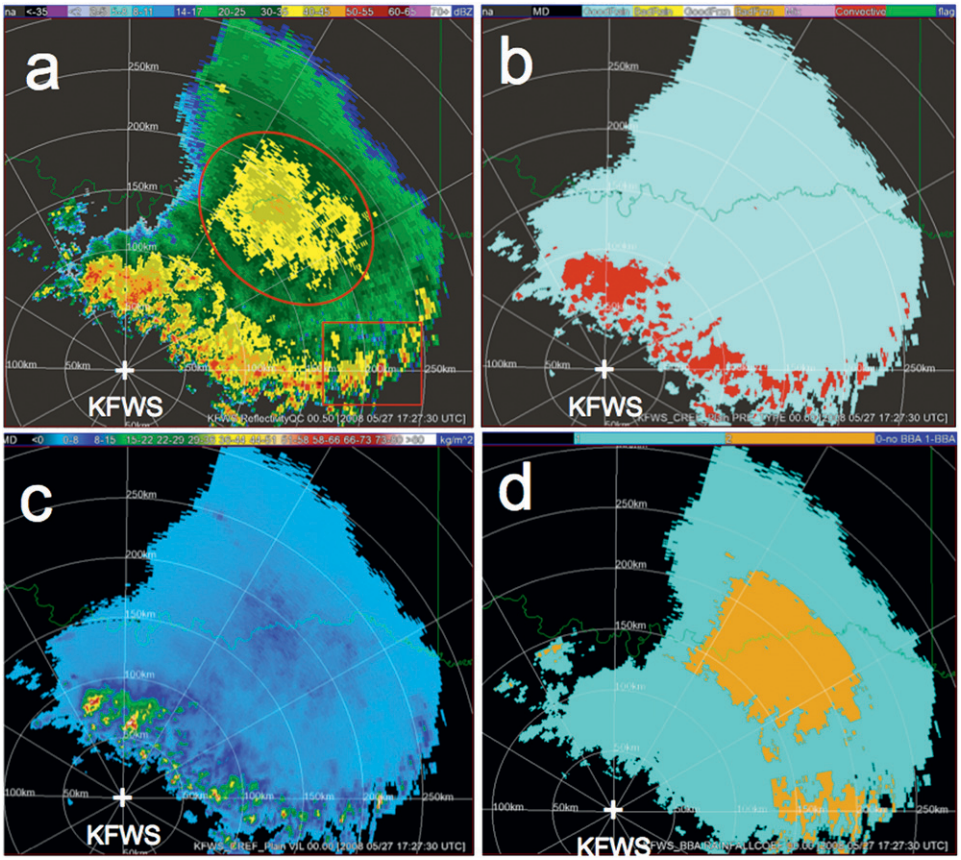

FIG. 2. (a) Base reflectivity on 0.5° tilt, (b) precipitation type, (c) VIL, and (d) the brightband affected area (BBA) fields from KFWS at 1727 UTC 27 May 2008. The red circle and squares in (a) indicates the area being affected by the brightband correction. The colors in (b) represent convective (red) and stratiform (blue) precipitation regions. The colors in (d) represent BBA (orange) and non-BBA (blue).

the precipitation is horizontally uniform. More specifically, it is assumed that the variation of reflectivity along a slant radial is dominated by the vertical gradient, especially in the brightband-affected regions:

$$Z_t(r, \varphi, \theta) \approx Z_t(\varphi, h). \tag{5}$$

Here $Z_t(r, \varphi, \theta)$ represents the true reflectivity at any given point in a spherical coordinate system (r = range, φ = azimuth, θ = elevation angle) originated from the radar; and h represents the height associated with (r, θ). Let $z_t(h)$ be the true VPR that is normalized by the reflectivity at the radar height, $Z_t(\varphi, 0)$, we have

$$Z_t(\varphi, h) = Z_t(\varphi, 0) z_t(h). \tag{6}$$

Then the radar observed ("apparent") reflectivity, $Z_a(\varphi, h)$, can be expressed as

$$Z_a(\varphi, h) = \int_{h-dh}^{h+dh} Z_t(\varphi, y) f^4(y)\, dy = Z_t(\varphi, 0) z_a(h), \tag{7a}$$

where

$$z_a(h) = \int_{h-dh}^{h+dh} z_t(y) f^4(y)\, dy; \tag{7b}$$

and $f^4(y)$ is the square of the normalized radar power gain pattern; dh is the half beamwidth at the height h on elevation angle θ; and $z_a(h)$ is the apparent VPR (AVPR). Rearranging Eq. (7a) and taking the log scale, we get an equation for the estimated reflectivity at the radar height:

$$\mathrm{dB}Z_t(\varphi, 0) = \mathrm{dB}Z_a(\varphi, h) - \mathrm{dB}z_a(h). \tag{8}$$

Figure 3 shows examples of $z_t(h)$ and $z_a(h)$ on the log scale assuming the WSR-88D radar beam characteristics. In the current study, the true VPR is assumed to be linear on the log scale with a zero slope below the brightband bottom (black solid line in Fig. 3), and the AVPR (gray dots in Fig. 3) is parameterized using a linear model (black dashed line in Fig. 3) with five parameters:

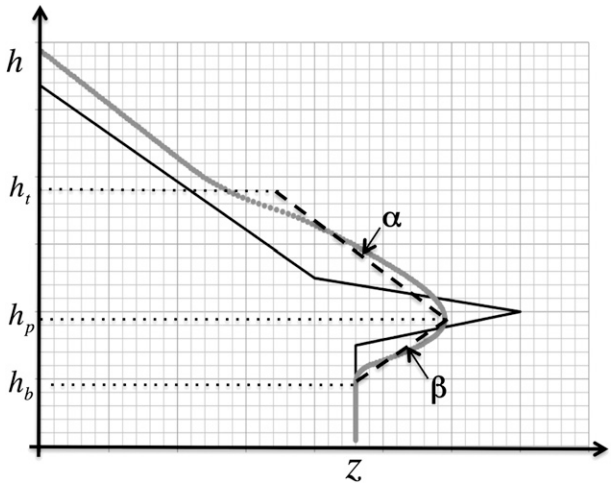

FIG. 3. Illustration of a true (black solid line) and an apparent (gray line) VPR. The apparent VPR is computed on 0.5° tilt assuming the WSR-88D radar beam characteristics. The black dashed line shows an idealized linear model fitted to the AVPR in the brightband-affected area. Definitions of the five parameters h_t, h_p, h_b, α, and β can be found in the text (section 2b).

1) Height of the apparent BB top (h_t) (ABT);
2) Height of the apparent BB bottom (h_b) (ABB);
3) Height of the apparent BB peak (h_p) (ABP);
4) Slope above the ABP (α);
5) Slope below the ABP (β);

For each tilt, the AVPR is computed by taking azimuthal average of reflectivities at each constant range within the BBA. This approach is different than most previous studies, where the mean VPR was derived using data at close ranges and from multiple tilts in a volume scan (e.g., Koistinen 1991; Joss and Lee 1995; Zhang et al. 2008). A quality control procedure is applied to exclude outliers and to assure a stable and representative AVPR. A valid mean reflectivity is obtained at a given range (height) only when there is sufficient number of BBA pixels at the range. The minimum number of pixels is a function of range (the farther the range, the less the number because the size of the pixels increases). Second, a running 15-point average in the vertical is applied to the AVPR, and any points that deviate more than twice the mean absolute deviation from the average are flagged as "bad." If more than 40% of the points in the AVPR were bad, then the AVPR is flagged as invalid. In this situation, a climate or predefined VPR could be used for correction. However, large uncertainties often result from such VPRs as they are usually associated with scattered or nonhomogeneous precipitation. Therefore, no correction is applied in the current study if a valid AVPR is not obtained.

The ABP(h_p) is defined as the height of the first maximum reflectivity below the ABT. Then the slope α is obtained by a least squares linear fitting to the AVPR between the ABT and ABP (Fig. 4). The ABB(h_b) is found by searching for the minimum reflectivity in the AVPR below the ABP. If the minimum reflectivity is lower than a threshold (default = 28 dBZ), then the height associated with the threshold is defined as h_b. The minimum reflectivity threshold is used to avoid excessive corrections. Once the ABB is found, the slope β is obtained by a least squares linear fitting to the AVPR between the ABP and ABT (Fig. 4). Note that α is always negative and β is always positive for a typical brightband structure. Otherwise, the precipitation is assumed to be a non-BB system and no correction is applied.

If the ABP is too close to the ground, then the ABB cannot be directly identified from the AVPR. Yet the correction is still needed because the overestimation is usually large under these circumstances (e.g., the third event in Fig. 1). Since many previous studies (e.g., Kitchen et al. 1994; Fabry and Zawadzki 1995; Sánchez-Diezma et al. 2000; Matrosov et al. 2007; Tabary 2007) have shown that a brightband VPR is approximately symmetric with respect to the peak, the AVPR is approximated by a symmetric model where $\alpha = \beta$ and $(h_t - h_p) = (h_p - h_b)$. Figure 4 shows that the AVPR fits the linear model very well for different events, especially below the ABB.

c. Apply correction

Once the parameterized AVPR is obtained, a log scale reflectivity correction factor, dB$z_a(h)$, is computed as the following:

$$\mathrm{dB}z_a(h) = \begin{cases} \alpha[h(r) - h_p] + \beta[h_p - h_b]; & h(r) > h_p \\ \beta[h(r) - h_b]; & h(r) \le h_p \end{cases}. \tag{9}$$

And the corrected reflectivity, dB$Z_c(\varphi, 0)$, is obtained according to Eq. (8):

$$\mathrm{dB}Z_c(\varphi, 0) = \mathrm{dB}Z_o(\varphi, h) - \mathrm{dB}z_a(h); \quad (\varphi, h) \in BBA. \tag{10}$$

Here, h, r, and φ are the height of the beam axis, range, and azimuth of a given gate, respectively; dB$Z_o(\varphi, h)$ represents the observed reflectivity (on log scale) at the gate.

For a brightband situation, dB$z_a(h)$ is usually positive, thus the correction would only reduce the observed reflectivities after the correction. It can become negative when $h(r) - h_p$ is so high that $\alpha[h(r) - h_p]$ is greater than

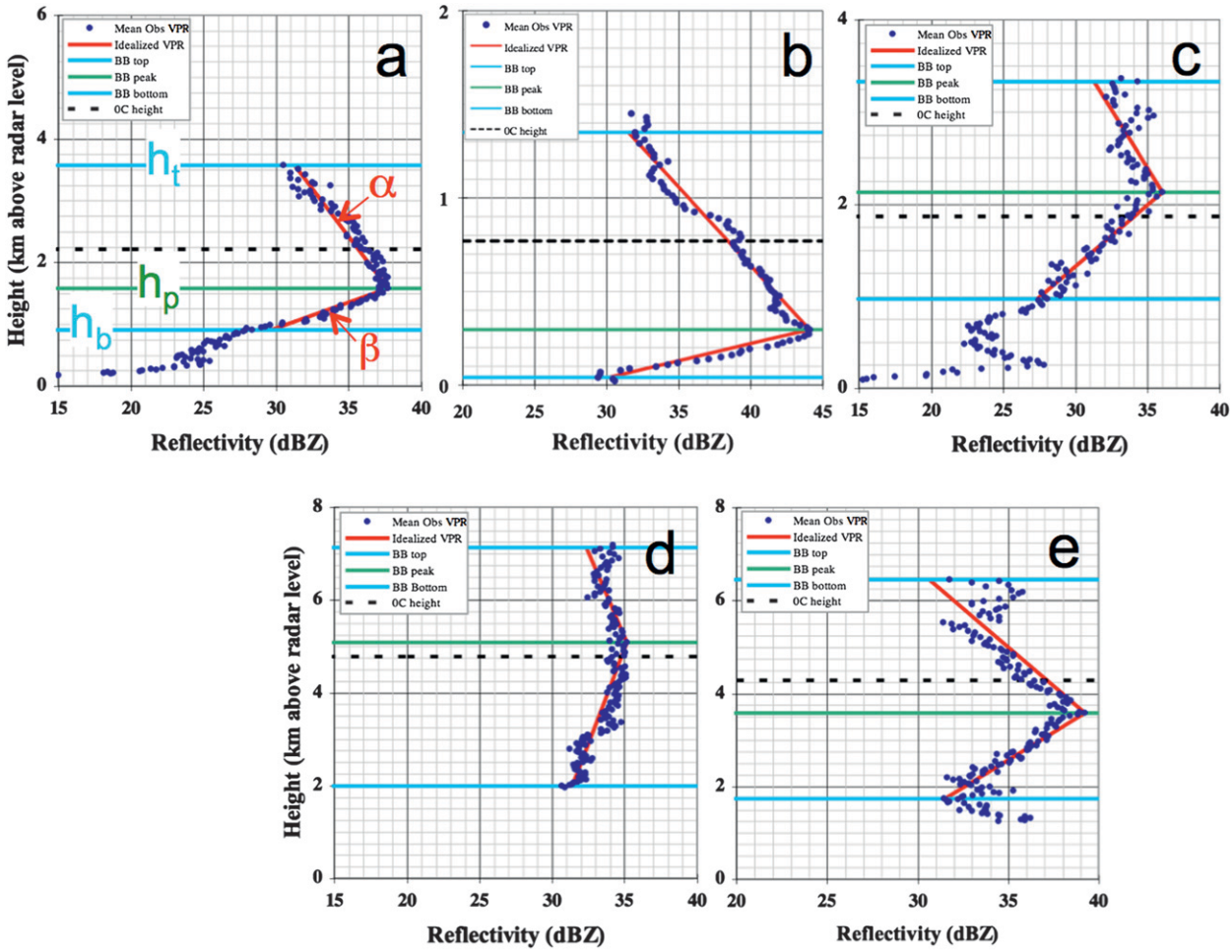

FIG. 4. Apparent VPRs (blue dots) and associated linear parameters (see text) for (a) KCLE at 1000 UTC 15 Nov 2008, (b) KUDX at 0500 UTC 27 May 2008, (c) KATX at 2004 UTC 7 Jan 2009, (d) KLZK at 1300 UTC 3 Sep 2008, and (e) KFWS at 1800 UTC 27 May 2008. Locations of the radars are shown in Fig. 1.

$\beta[h_p - h_b]$, and Eq. (10) may be potentially used to correct for underestimations in radar-derived QPEs when the radar beam is sampling upper part of precipitation clouds (i.e., the ice region). However, this correction may not be very accurate if only one slope is considered above the BB peak. A second piece of linear fitting scheme may be necessary for more accurate representation of the ice region above the ABT. Furthermore, previous studies (e.g., Seo et al. 2000; Germann and Joss 2002) indicated that such attempts would only be useful when the radar coverage was good. The correction for the ice region will be an extension of the current study and is beyond the scope of this paper.

In the current study, multiple AVPRs are derived and then applied for correction, one for each tilt. The correction is applied to reflectivities at the corresponding ranges where the AVPR was computed, accounting for the beam-broadening effect implicitly. Since the correction was only applied down to the ABB, the beam-broadening effect was only corrected up to this range. Nevertheless, if the true VPR slope is near zero below the BB bottom, then the AVPR is almost identical to the true VPR below the ABB (Fig. 3). This was also shown in the study of Sánchez-Diezma et al. (2000). Thus, the current method should correct majority of radar QPE errors caused by a bright band. This approach was found to be superior to the single-VPR approach, where one mean VPR is computed from observations of multiple elevations angles at closer ranges and then applied to the far ranges. Experiments with the single-VPR approach resulted in some circular discontinuities (not shown) because the VPRs could not accurately account for the beam broadening at different ranges. Using the AVPRs from each tilt, the correction is adaptive to the actual beam-broadening effects and the BB distribution in the specific atmospheric environment, and discontinuities in

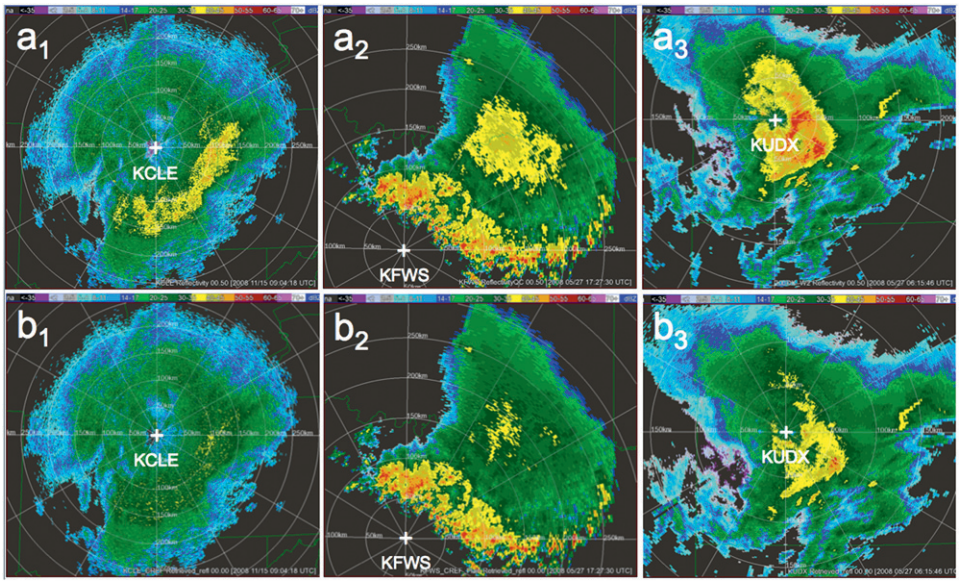

FIG. 5. Base-level reflectivities on the lowest tilt (row a) before and (row b) after the AVPR correction. Images from (left) KCLE at 1000 UTC 15 Nov 2008, (middle) KFWS at 1800 UTC 27 May 2008, and (right) KUDX at 0500 UTC 27 May 2008.

the corrected fields are minimized. Figure 5 shows example reflectivity fields before and after the AVPR correction. The inflated reflectivities in the brightband area were corrected. The corrected fields showed physically continuous distributions and were free of circular discontinuities that are usually caused by unrepresentative BB top/bottom heights in single-VPR approaches. The correction to the KUDX reflectivity field (Fig. 5c) appeared to be insufficient and a strong echo band remained in the southeast of the radar. This was probably due to a second melting level as indicated by a second and higher 0°C level in the atmospheric sounding (at ~1.25 km above the radar level). And further studies on this type of precipitation are needed.

d. *Constructing hybrid scan reflectivity*

There are nine operational volume scan modes, or volumes scan patterns (VCPs), in the current WSR-88D network [(National Oceanic and Atmospheric Administration/Office of the Federal Coordinator for Meteorological Services and Supporting Research) NOAA/OFCM 2005]. The number of tilts in a volume scan ranges from 5 to 14 for different VCPs (Table 1). To construct a hybrid scan reflectivity field for precipitation

TABLE 1. List of the operational WSR-88D volume scan strategies.

VCP ID	No. of tilts	Scan cycle (min)	Elevation angles (°)	Remarks
11	14	5	0.5, 1.45, 2.4, 3.35, 4.3, 5.25, 6.2, 7.5, 8.7, 10.0, 12.0, 14.0, 16.7, 19.5	Used for convections, especially when close to the radar
21	9	6	0.5, 1.45, 2.4, 3.35, 4.3, 6.0, 9.9, 14.6, 19.5	Used for convections (not used often since VCP12 become available)
31	5	10	0.5, 1.5, 2.5, 3.5, 4.5	Long pulse used for detecting subtle boundaries and winter precipitation
32	5	10	Same as VCP 31	Short pulse for less velocity ambiguity. Default clear air mode
12	14	4.1	0.5, 0.9, 1.3, 1.8, 2.4, 3.1, 4.0, 5.2, 6.4, 8.0, 10.0, 12.5, 15.6, 19.5	For convections, especially at long ranges
121	9	6	Same as VCP 21	Scan lower elevation angles multiple times with varying pulse repetitions to get better velocity data
211	14	5	Same as VCP 11	Reduced range ambiguity and often used for large tropical systems (hurricanes)
212	14	4.1	Same as VCP 12	
221	9	9	Same as VCP 21	

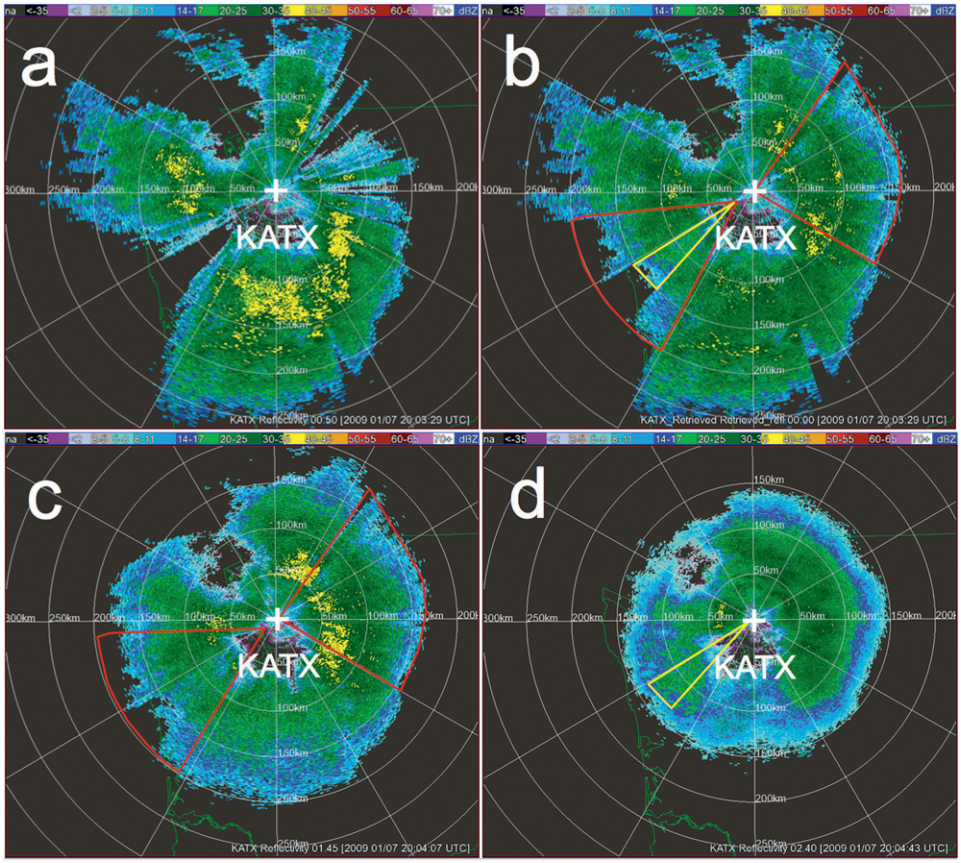

FIG. 6. Base-level reflectivities on the (a) 0.5°, (c) 1.45°, and (d) 2.4° tilts and (b) the hybrid scan reflectivity from KATX at 2004 UTC 7 Jan 2009. The red and yellow outlined areas were the corrected reflectivities from 1.45° and 2.4° tilts, respectively.

estimation, an AVPR is computed and then the correction is applied to the lowest tilt first. If there are areas in the lowest tilt with more than 50% (an adaptable parameter) blockages, then an AVPR is computed and the correction is applied on the second-lowest tilt. This procedure is repeated for higher elevation angles until there are no blockages higher than the threshold can be found. Then a hybrid scan reflectivity (HSR) field is constructed using the AVPR corrected reflectivity from the lowest "unblocked" (i.e., <50%) gates among the multiple tilts. Figure 6 shows the raw base reflectivities on the lowest three tilts (Figs. 6a,c,d) from KATX radar at 2004 UTC 7 January 2009 and a hybrid scan reflectivity (Fig. 6b) constructed from the corrected reflectivities on the three tilts. There was evident bright band in both the first and second tilts (Figs. 6a,c). However, the BB structure was not as well defined as in the flatland cases (e.g., Fig. $5a_1$) due to the impact of complex terrains. The areas outlined with red and yellow lines in the hybrid scan reflectivity (Fig. 6b) indicate contributions from the second and third tilts, respectively.

The hybrid scan provided better depictions of precipitation than the lowest tilt in the areas to the southwest and east-northeast of the radar (Figs. 6b vs. 6a). Furthermore, the correction reduced BB contaminations in the first and second tilts and resulted in a uniformly distributed precipitation. There were still discontinuities to the southwest of the radar due to severe blockages. The echo coverage clearly showed limited radar visibilities in this region. Beyond a range of ~150 km, any VPR correction efforts would be futile because there were no valid reflectivity measurements available from any tilts. This is a very challenging issue for radar-derived QPEs in mountainous areas (e.g., Kitchen et al. 1994; Seo et al. 2000; Pellarin et al. 2002; Germann and Joss 2002; Tabary et al. 2007). Additional sensors such as rain gauge, satellite, or gap-filling X-band polarimetric Doppler radars (Gourley et al. 2009) and methodologies incorporating local precipitation characteristics (e.g., DiLuzio et al. 2008; Daly et al. 2007a,b) are needed to further improve radar precipitation estimation.

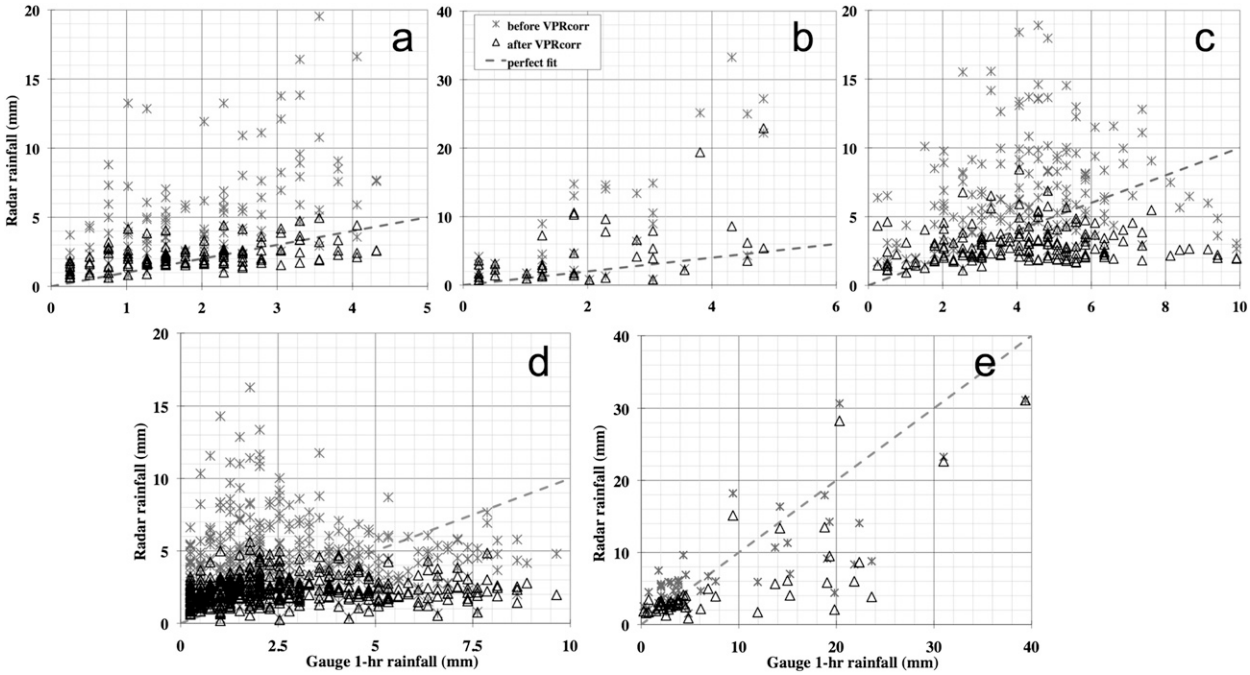

FIG. 7. Scatterplots of 1-h radar precipitation estimates before (stars) and after (triangles) the AVPR correction vs gauge observations. The data are from (a) KCLE 0500–1000 UTC 15 Nov 2008, (b) KUDX 0000–0900 UTC 27 May 2008, (c) KATX 1400 UTC 7 Jan to 1600 UTC 8 Jan 2009, (d) KLZK 0000–1200 UTC 3 Sep 2008, and (e) KFWS 1300–2000 UTC 27 May 2008.

3. Case study results

In the current study, the hybrid scan reflectivity field is converted into rain rate using two Z–R relationships: one for convective areas ($Z = 300R^{1.4}$) and another one for stratiform areas ($Z = 200R^{1.6}$). The rain rates are aggregated into hourly rainfalls and compared to the surface gauge observations. Figure 7 shows a comparison of hourly radar rainfall estimates before and after the AVPR correction against gauge observations for the five events shown in Fig. 1. The significant overestimations in radar-derived QPE of the KCLE (Fig. 7a), KUDX (Fig. 7b), KATX (Fig. 7c), and KLZK (Fig. 7d) were successfully reduced by the correction. Radar estimates after the correction agreed much better with the gauge observations than those before, especially for the amounts less than 5 mm. For the squall-line event (Fig. 7e), the imperfect convective–stratiform segregation resulted in erroneous reductions of the higher amounts (e.g., those >10 mm). For the Hurricane Gustav event (Fig. 7d), there was evident underestimation in radar-derived QPEs before the AVPR correction for the heavy amounts (e.g., those greater than 5 mm). We hypothesize that the Z–R relationships used in the current study ($Z = 300R^{1.4}$ and $Z = 200R^{1.6}$) were not representative of the high-efficiency tropical warm rain process in this event. In the real-time system, a tropical-precipitation identification (Xu et al. 2008) will be applied and a more proper Z–R relationship will be used to mitigate the underestimation.

A more extensive evaluation of the BB correction scheme was performed using eight heavy precipitation events from different regions and seasons in the United States (Table 2). Hourly gauge data from the Hydrometeorological Automated Data System (HADS; see online at http://www.nws.noaa.gov/oh/hads/) are used in the current study for evaluations of the AVPR correction. The data for the 8 events included 2467 hourly HADS gauges and 268 h of volume scan data from 18 radars (Table 2). Three statistic scores were used to assess the performance of the correction scheme.

1) Root-mean-square error (RMSE):

$$\mathrm{RMSE} = \left[\frac{1}{N}\sum_{k=1,N}(r_k - g_k)^2\right]^{1/2}. \qquad (11)$$

Here r_k and g_k represent the kth matching pair of the radar-derived and gauge observed rainfall in the BBA; N represents the total number of matching gauge and radar pixel pairs in the BBA. A matching pair of gauge and radar pixel is found when the following two criteria are met: (i) the gauge location is within the boundary of a $1° \times 1$ km radar bin, and (ii) both the radar estimate r_k and the gauge observation g_k are greater than 0.

TABLE 2. Summary of the events.

Events	Radar	No. of radar–gauge pairs	Time and date	Event summary
1	KUDX (44.12°N, 102.83°W)	48	0000–0900 UTC 27 May 2008	Stratiform, BB near the ground
2	KFWS (32.57°N, 97.30°W)	49	1200–2000 UTC27 May 2008	Convective, melting snow aggregates in the trailing precipitation behind a squall line
	KSRX (35.29°N, 94.36°W)	100		
	KTLX (35.33°N, 97.27°W)	108		
3	KLZK (34.83°N, 92.26°W)	446	0000–1600 UTC 3 Sep 2008	Tropical rain to the south and west of the radar, BB to the northeast
4	KILN (39.42°N, 83.82°W)	156	0000–1200 UTC 15 Nov 2008	Stratiform, well-defined BB in VPRs
	KPBZ (40.53°N, 80.21°W)	172		
	KCLE (41.41°N, 81.86°W)	122		
5	KATX (48.19°N, 122.49°W)	173	1400 UTC 7 Jan 2009–1600 UTC 8 Jan 2009	Stratiform with BB in complex terrain, mixed with orographic rain
6	KSRX (35.29°N, 94.36°W)	111	1200 11 Mar 2009–1200 UTC 12 Mar 2009	Stratiform, well-defined BB in VPRs, Blockages in KSRX data
	KFWS (32.57°N, 97.30°W)	274		
	KLZK (34.83°N, 92.26°W)	197		
	KSHV (32.45°N, 93.84°W)	174		
7	KAMA (35.23°N, 101.70°W)	11	0400–1100 UTC 9 Feb 2009	Convective, melting snow aggregates in the trailing precipitation behind a squall line
	KFDR (34.36°N, 98.97°W)	45		
	KLBB (33.65°N, 101.81°W)	16		
	KMAF (31.94°N, 102.19°W)	7		
8	KDAX (38.50°N, 121.67°W)	163	0300 1 Nov 2008–1200 UTC 2 Nov 2008	Stratiform with BB in complex terrain, mixed with orographic rain
Tot	18* radars	2467 radar–gauge pairs	268 h	8 events

* Some radars are counted more than once because they appeared in multiple events.

2) Relative mean absolute error (RMAE):

$$\mathrm{RMAE} = \frac{\frac{1}{N}\sum_{k=1,N}|r_k - g_k|}{\overline{G}}, \tag{12a}$$

$$\overline{G} = \frac{1}{N}\sum_{k=1,N} g_k. \tag{12b}$$

Here $\overline{G}$ is the averaged hourly gauge precipitation.

3) Relative Mean Bias (RMB):

$$\mathrm{RMB} = \frac{\frac{1}{N}\sum_{k=1,N}(r_k - g_k)}{\overline{G}}. \tag{13}$$

Figure 8 shows the three statistic scores of the radar hourly rainfall estimates with respect to the HADS observations for 18 radars and 8 events. The AVPR correction consistently reduced the radar-derived QPE errors for all the events except for one (KDAX 20081101), which was an event from a complex terrain. The improvements were most significant for the two events (KUDX 20080527 and KAMA 20090209; Fig. 8) where the bright band were near the ground. Large improvements were also found for the cool season stratiform precipitation in the northeast (KCLE, KILN, and KPBZ 20081115) and in the Great Plains (KSRX and KLZK 20090311). The relative small improvement in the RMAE for KFWS 20080527 event, and in RMB scores for KLBB20090209, KMAF, and KFWS20090311 events were due to the imperfect convective–stratiform segregation as mentioned earlier in this paper (see section 2).

4. Summary and future work

A real-time algorithm for the correction of bright-band (BB) effects in radar precipitation estimation was developed. The correction was based on the radar observed ("apparent") vertical profiles of reflectivity (AVPRs) from volumetric radar data. The AVPR was computed for each single tilt, and only in the bright-band area that was delineated according to radar reflectivity distributions and atmospheric environmental data. A linear model was fitted to the AVPR and then used to correct for BB effects in the observed reflectivity field.

The AVPR correction scheme was tested for eight heavy precipitation events from different geographical regions and seasons in the United States. The linear VPR model was found to be representative and stable for various BB structures. High reflectivities associated with BB were correctly reduced in most of the cases and the corrected reflectivity field showed physically continuous distributions. The overestimation errors in radar-derived QPE were largely reduced after the correction,

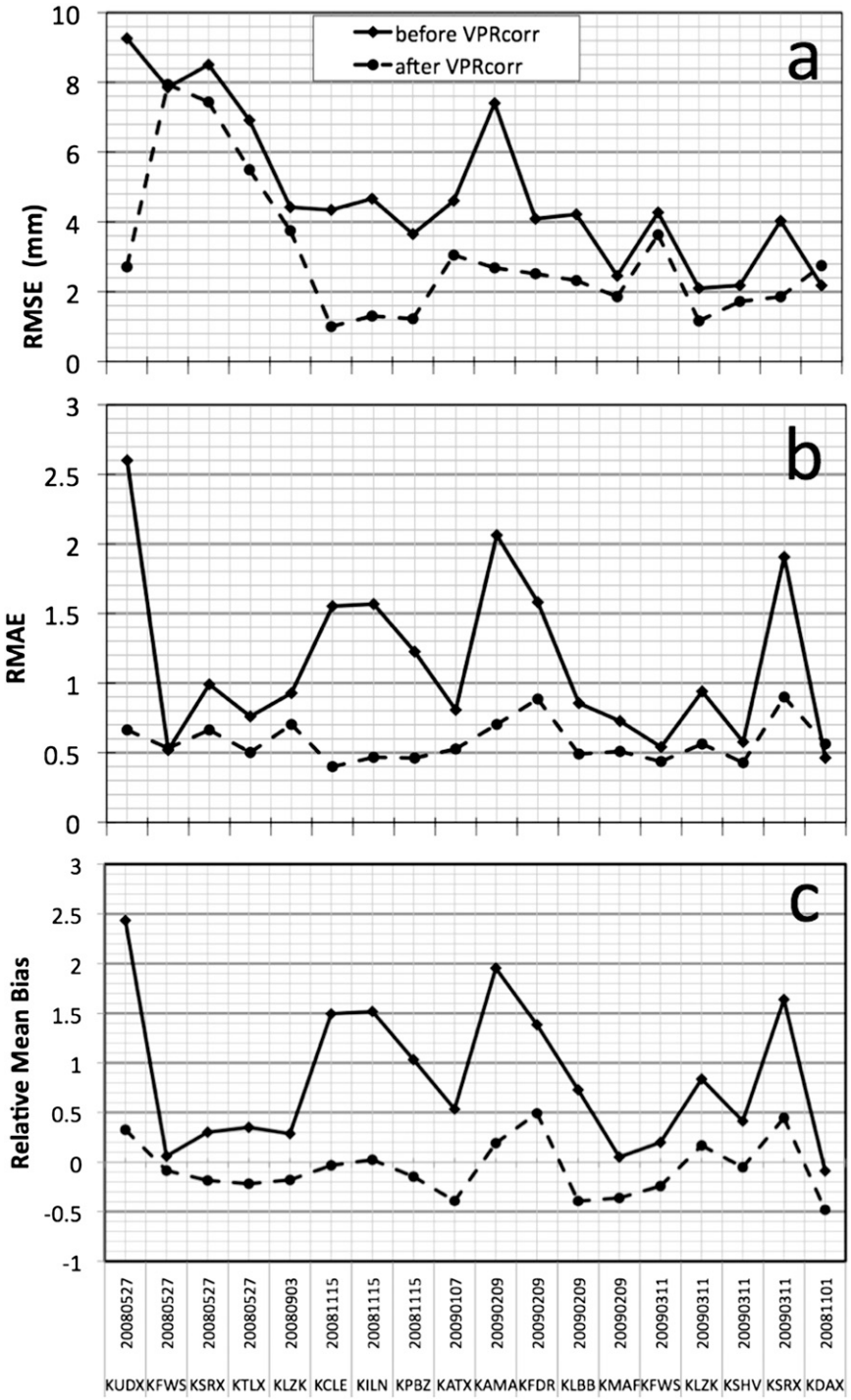

FIG. 8. The (a) RMSE, (b) relative MAE, and (c) relative bias scores for radar precipitation estimates before (solid line) and after (dashed line) the AVPR correction.

and the corrected radar-derived QPE agreed well with rain gauge observations. The AVPR correction is most effective and robust for flat land radars because of relative uniform spatial distributions of BB. For mountainous radars, the performance of the correction is mixed because of large spatial variations of VPRs caused by underlying topography. The current convective–stratiform segregation still needs further refinement. And delineations of tropical and orographically enhanced rain from the BB-impacted stratiform precipitation are very important.

Future work will include refinements of the convective–stratiform segregation and the apparent BB top and bottom heights calculations. Evaluations of the correction scheme will be expanded as it is implemented in the NMQ system. The AVPR correction for radar precipitation above the BB top will be explored. Furthermore, the integration of the current AVPR correction algorithm and dual-polarization radar-derived QPE techniques will be investigated.

Acknowledgments. Major funding for this research was provided under NOAA's Hydro-Meteorological Testbed (HMT) program and partial funding was provided under NOAA–University of Oklahoma Cooperative Agreement NA17RJ1227. The authors thank Kenneth Howard for many insightful discussions during this study. This manuscript has greatly benefited from the comments of anonymous reviewers, and from the comments of Drs. David Jorgensen, J. J. Gourley, Alexander Ryzhkov, and David Kingsmill.

REFERENCES

Andrieu, H., and J. D. Creutin, 1995: Identification of vertical profiles of radar reflectivity for hydrological applications using an inverse method. Part I: Formulation. *J. Appl. Meteor.,* **34,** 225–239.

Austin, P. M., and A. C. Bemis, 1950: A quantitative study of the "bright band" in radar precipitation echoes. *J. Meteor.,* **7,** 145–151.

Bellon, A., G.-W. Lee, and I. Zawadzki, 2005: Error statistics of VPR corrections in stratiform precipitation. *J. Appl. Meteor.,* **44,** 998–1015.

Daly, C., W. P. Gibson, G. H. Taylor, M. K. Doggett, and J. I. Smith, 2007a: Observer bias in daily precipitation measurements at U.S. Cooperative network stations. *Bull. Amer. Meteor. Soc.,* **88,** 899–912.

——, J. I. Smith, and R. McKane, 2007b: High-resolution spatial modeling of daily weather elements for a catchment in the Oregon Cascade Mountains, United States. *J. Appl. Meteor. Climatol.,* **46,** 1565–1586.

DiLuzio, M., G. L. Johnson, C. Daly, J. K. Eischeid, and J. G. Arnold, 2008: Constructing retrospective gridded daily precipitation and temperature datasets for the conterminous United States. *J. Appl. Meteor. Climatol.,* **47,** 475–497.

Fabry, F., and I. Zawadzki, 1995: Long-term radar observations of the melting layer of precipitation and their interpretation. *J. Atmos. Sci.,* **52,** 838–851.

Germann, U., and J. Joss, 2002: Mesobeta profiles to extrapolate radar precipitation measurements above the Alps to the ground level. *J. Appl. Meteor.,* **41,** 542–557.

Gourley, J. J., and C. Calvert, 2003: Automated detection of the bright band using WSR-88D data. *Wea. Forecasting,* **18,** 585–599.

——, D. P. Jorgensen, S. Y. Matrosov, and Z. L. Flaming, 2009: Evaluation of incremental improvements to quantitative precipitation estimates in complex terrain. *J. Hydrometeor.,* **10,** 1507–1520.

Greene, D. R., and R. A. Clark, 1972: Vertically integrated liquid water—A new analysis tool. *Mon. Wea. Rev.,* **100,** 548–552.

Joss, J., and R. Lee, 1995: The application of radar-gauge comparisons to operational precipitation profile corrections. *J. Appl. Meteor.,* **34,** 2612–2630.

Kitchen, M., 1997: Towards improved radar estimates of surface precipitation at long range. *Quart. J. Roy. Meteor. Soc.,* **123,** 145–163.

——, R. Brown, and A. G. Davies, 1994: Real-time correction of weather radar data for the effects of bright band, range and orographic growth in widespread precipitation. *Quart. J. Roy. Meteor. Soc.,* **120,** 1231–1254.

Koistinen, J., 1991: Operational correction of radar rainfall errors due to the vertical reflectivity profile. Preprints, *25th Int. Conf. on Radar Meteorology,* Paris, France, Amer. Meteor. Soc., 91–94.

Lhermitte, R. M., and D. Atlas, 1963: Doppler fall speed and particle growth in stratiform precipitation. Preprints, *10th Radar Meteorology Conf.,* Washington, DC, Amer. Meteor. Soc., 297–302.

Matrosov, S. Y., K. A. Clark, and D. E. Kingsmill, 2007: A polarimetric radar approach to identify rain, melting-layer, and snow regions for applying corrections to vertical profiles of reflectivity. *J. Appl. Meteor. Climatol.,* **46,** 154–166.

NOAA/OFCM, 2005: Surface weather observations and reports. Federal Meteorological Handbook 11, FCM-H1-2005, NOAA/Office of the Federal Coordinator for Meteorological Services and Supporting Research, Washington, DC, 104 pp. [Available online at http://www.ofcm.gov/homepage/text/pubs.htm.]

Pellarin, T., G. Delrieu, G.-M. Saulnier, H. Andrieu, B. Vignal, and J.-D. Creutin, 2002: Hydrologic visibility of weather radar systems operating in mountainous regions: Case study for the Ardèche catchment (France). *J. Hydrometeor.,* **3,** 539–555.

Ryde, J. W., 1947: The attenuation and radar echoes produced at centimeter wavelengths by various meteorological phenomena. *Meteorological Factors in Radio Wave Propagation,* The Physical Society, 169–188.

Sánchez-Diezma, R., I. Zawadzki, and D. Sempere-Torres, 2000: Identification of the bright band through the analysis of volumetric radar data. *J. Geophys. Res.,* **105,** 2225–2236.

Seo, D.-J., J. Breidenbach, R. Fulton, D. Miller, and T. O'Bannon, 2000: Real-time adjustment of range-dependent biases in WSR-88D rainfall estimates due to nonuniform vertical profile of reflectivity. *J. Hydrometeor.,* **1,** 222–240.

——, C. R. Kondragunta, K. Howard, S. V. Vasiloff, and J. Zhang, 2005: The national mosaic and multisensor QPE (NMQ) project-status and plans for a community testbed for high-resolution multisensor quantitative precipitation estimation (QPE) over the United States. Preprints, *19th Conf. on Hydrology,* San Diego, CA, Amer. Meteor. Soc., P1.3.

Smyth, T. J., and A. J. Illingworth, 1998: Radar estimates of rainfall rates at the ground in bright band and non-bright band events. *Quart. J. Roy. Meteor. Soc.,* **124,** 2417–2434.

Steiner, M., R. A. Houze Jr., and S. E. Yuter, 1995: Climatological characterization of three-dimensional storm structure from operational radar and rain gauge data. *J. Appl. Meteor.,* **34,** 1978–2007.

Tabary, P., 2007: The new French operational radar rainfall product. Part I: Methodology. *Wea. Forecasting,* **22,** 393–408.

——, J. Desplats, K. Do Khac, F. Eideliman, C. Gueguen, and J.-C. Heinrich, 2007: The new French operational radar rainfall product. Part II: Validation. *Wea. Forecasting,* **22,** 409–427.

Vasiloff, S., and Coauthors, 2007: Q2: Next generation QPE and very short-term QPF. *Bull. Amer. Meteor. Soc.,* **88,** 1899–1911.

Vignal, B., and W. F. Krajewski, 2001: Large-sample evaluation of two methods to correct range-dependent error for WSR-88D rainfall estimates. *J. Hydrometeor.,* **2,** 490–504.

——, H. Andrieu, and J. D. Creutin, 1999: Identification of vertical profiles of reflectivity from volume-scan radar data. *J. Appl. Meteor.,* **38,** 1214–1228.

——, G. Galli, J. Joss, and U. Germann, 2000: Three methods to determine profiles of reflectivity from volumetric radar data to correct precipitation estimates. *J. Appl. Meteor.,* **39,** 1715–1726.

Westrick, K. J., C. F. Mass, and B. A. Colle, 1999: The limitations of the WSR-88D radar network for quantitative precipitation measurement over coastal western United States. *Bull. Amer. Meteor. Soc.,* **80,** 2289–2298.

Wexler, R., and D. Atlas, 1956: Factors influencing radar echo intensities in the melting layer. *Quart. J. Roy. Meteor. Soc.,* **82,** 349–351.

Xu, X., K. Howard, and J. Zhang, 2008: An automated radar technique for the identification of tropical precipitation. *J. Hydrometeor.,* **9,** 885–902.

Zhang, J., C. Langston, and K. Howard, 2008: Bright band identification based on vertical profiles of reflectivity from the WSR-88D. *J. Atmos. Oceanic Technol.,* **25,** 1859–1872.